rspa.royalsocietypublishing.org

Palæotsunamis and tsunami hazards in the Eastern Mediterranean

Philip England[1], Andrew Howell,[2] James Jackson[2] and Costas Synolakis[3,4]

[1]Department of Earth Sciences, University of Oxford, South Parks Road, Oxford OX1 3AN, UK
[2]Department of Earth Sciences, Bullard Labs, Madingley Road, Cambridge CB3 0EZ, UK
[3]Department of Environmental Engineering, Technical University of Crete, Chania, Greece
[4]Viterbi School of Engineering, University of Southern California, Los Angeles, CA 90089-2531, USA

Research

Article submitted to journal

Subject Areas:
Natural Hazards, Geology, Geophysics

Keywords:
Tsunami, Earthquake, East Mediterranean

Author for correspondence:
Philip England
e-mail:
Philip.England@earth.ox.ac.uk

The dominant uncertainties in assessing tsunami hazard in the Eastern Mediterranean are attached to the location of the sources. Reliable historical reports exist for five tsunamis associated with earthquakes at the Hellenic plate boundary, including two that caused widespread devastation. Because most of the relative motion across this boundary is aseismic, however, the modern record of seismicity provides little or no information about the faults that are likely to generate such earthquakes. Independent geological and geophysical observations of two large historical-to-prehistorical earthquakes, in Crete and Rhodes, lead to a coherent framework in which large to great earthquakes occurred not on the subduction boundary, but on reverse faults within the overlying crust. We apply this framework to the less complete evidence from the remainder of the Hellenic plate boundary zone, identifying candidate sources for future tsunamigenic earthquakes. Each such source poses a significant hazard to the North African coast of the Eastern Mediterranean. Because modern rates of seismicity are irrelevant to slip on the tsunamigenic faults, and because historical and geological data are too sparse, there is no reliable basis for a probabilistic assessment of this hazard, and a precautionary approach seems advisable.

1. Introduction

The assessment of tsunami hazard in the Eastern Mediterranean has been severely hampered by uncertainty in the locations and magnitudes of the causative earthquakes; in consequence a wide range of calculated scenarios exists for tsunamigenic earthquakes in the region (*e.g.* [1–5]). The two most devastating historical tsunamis recorded in the region, those of AD 365 and AD 1303, were probably generated by large or great (magnitude $\gtrsim 7$ or magnitude > 8) earthquakes at the Hellenic plate boundary (*e.g.* [6,7]). There is strong geological evidence that the AD 365 tsunami was caused by an earthquake in Western Crete (*e.g.* [8–12]) and that another tsunamigenic earthquake occurred near Rhodes in prehistorical or Roman times [13–16]. Attempts to identify other source locations along the Hellenic plate boundary have relied on analogies with major subduction zones around the world, and have defined source parameters on the basis of the seismicity of the past few decades. The complexity of this plate boundary zone, and the fact that most of the convergence across it is aseismic [17], suggest that the seismicity data, alone, are a misleading guide to likely sources of tsunamigenic earthquakes. Instead, we develop a model that takes advantage of recent understanding of the tsunami hazard at this plate boundary which has developed by combining geological, geophysical, geodetic, geomorphological, geochronological, and historical data. (*e.g.* [10,12,13,18–21]).

2. Tectonic Setting

The Hellenic plate boundary zone accommodates ~ 40 mm/yr of relative motion between the oceanic lithosphere of the Eastern Mediterranean (part of the Nubian plate) and continental lithosphere of Greece and the Aegean Sea [21–23]. Approximately three-quarters of this motion arises from distributed deformation within the continental lithosphere of Greece and Turkey, which causes the southern Aegean to move southwestwards with respect to stable Eurasia at $\sim$30 mm/yr [24,25]. The lithosphere of the Aegean region undergoes horizontal extension, as is shown by pervasive normal faulting (Figure 1a, and see [26]). In the southernmost Aegean, earthquakes, active faulting, and GPS data show along-arc extension (Figure 1, and see [19,20,27–29]) which, combined with the change in strike of the plate boundary zone from NW-SE in the west to almost SW-NE in the east, causes the relative motion across the boundary to vary from from almost pure convergence in the west to highly oblique convergence in the east (Figure 1b).

Studies of the release of seismic moment in the region over the instrumental period [17] and of the relative motions recorded by GPS measurements [21] suggest that less than 20% of the relative motion takes place in earthquakes, with the remainder taking place by aseismic slip. To accommodate the relative motion seismically would require a M8 earthquake approximately once per century and, although the historical record is incomplete, it is inconceivable that the ~ 20 great earthquakes that would be needed to remove the deficit during the past 2,000 years could have occurred unremarked [6,17]. But the historical record does indicate that two or three great earthquakes occurred at this boundary during this interval of time [6]. Because there is no known place where a fault that slips predominantly aseismically also fails in occasional great earthquakes, the logical conclusion to draw is that great earthquakes in the Hellenic plate boundary zone occur not on the subduction fault but on another fault or faults within the zone [10].

The complex morphology of the region makes the identification of those faults difficult. Most subduction zones exhibit a steep-sided bathymetric low, the trench, which marks the projection to the surface of the subduction fault. The subduction fault in the Hellenic plate boundary zone does not crop out; its closest approach to the surface probably lies beneath the broad bathymetric high of the Mediterranean Ridge (Figure 1), a prism of sediments about 10 km thick [35–37]. Deep ($\sim$ 4,000m below sea level) linear features are, however, visible in the bathymetry of the Hellenic plate boundary, in particular the Hellenic, Pliny, and Strabo Trenches (Figure 1a). These features are not, despite their names, trenches in the plate-tectonic sense but probably represent the outcrop of major faults within the deforming sedimentary wedge on top of the Nubian plate [10,20,36,38–41]. While the Hellenic Trench is generally considered to represent the outcrop of a reverse fault, the Pliny and Strabo Trenches (Figure 1a) have been interpreted as the expressions of normal faulting [42], strike-slip faulting [43,44], reverse faulting [20,45], and various combinations of these (*e.g.* [36,40,46,47]).

The bathymetric profiles across the Hellenic, Pliny, and Strabo Trenches, and across the north edge of the Rhodes Basin, show strong similarities that suggest these features may have a common origin (Figure 2). In each case, the depth of the ocean floor increases northwards of the Mediterranean Ridge towards the trenches, with maximum depths of 3,000 m to 4,500 m occurring close to the continental margin of the Peloponnese and the Aegean Sea. The profiles are also strongly asymmetric, with steep slopes on the landward sides, a form that is characteristic of topographic profiles perpendicular to major reverse faults. The similarities between the profiles are paradoxical because the direction of overall relative motion across this region varies from pure convergence in the west to highly oblique in the east (Figure 1b). *Howell et al.* [13] suggest that the paradox may be resolved if relative motion across the eastern part of the plate boundary is partitioned into arc-parallel slip along the subduction interface and arc-perpendicular reverse faulting that crops out on the trenches within the over-riding Aegean crust (Figure 3).

This suggestion is supported by the slip vectors of the few earthquakes along the subduction fault for which focal mechanisms may be determined [13,20,48], and by the relative velocities of GPS sites in the southernmost Aegean ([21–23,25], Figure 1b). While baselines parallel to the trench system are generally extending, consistent with the observations of active faulting and focal mechanisms of earthquakes (Figure 1 and see [19,27]), baselines perpendicular to the trenches are generally shortening. Thus, a small fraction of the convergence rate between the Aegean and Nubia is being accommodated by contractional strain within the Aegean lithosphere [10,21]. In Section 3 we discuss the evidence suggesting that this contraction is eventually released in occasional large or great earthquakes on reverse faults whose outcrops are marked by the Hellenic, Pliny, and Strabo trenches (Figures 1 and 3). In Section 4 we carry out hydrological simulations of candidate tsunamis generated by such sources.

3. Potential tsunami sources at the Hellenic plate boundary

(a) Historical record

The assessment of tsunami hazard in the Eastern Mediterranean is hampered by the proliferation of tsunami catalogues, many of which are based on secondary or more distant sources, and which have promulgated a range of errors, including non-existent earthquakes and tsunamis. Comparing these catalogues with the historical record, *Ambraseys and Synolakis* [7] rejected 65 out of 75 alleged historic tsunamis between AD 66 and 1928. Half of the historical reports rejected by *Ambraseys and Synolakis* [7] were either not based on historical sources, or the sources had been interpreted "with a tinge of imagination". The remaining incorrect attributions of tsunamis represent inundations that were probably caused by local effects, including storm surges (see, also, [49]). We refer the reader to detailed analysis of the historical record [6,7,49] for a wider discussion of the pitfalls in its interpretation.

Five reliable historical reports of tsunamis are closely associated with earthquakes along the Hellenic plate boundary: 21st July AD 365, Crete; 8 August AD 1303, Crete; 3rd May AD 1481, Rhodes; 28th February AD 1629, Kithyra; 22nd January, AD 1899, Kyparissia. The approximate locations of these events are shown in Figure 1b.

(b) The AD 365 earthquake and tsunami

The historical evidence for devastation of Alexandria and surrounding regions by a tsunami on 21 July AD 365 is well established [6,50,51]. The tsunami has long been attributed, on the basis of uplifted indicators of past sea level or 'sea marks', to an earthquake whose epicentre lay near Western Crete (*e.g.* [9,11,12,52,53]). Recent analysis shows that these observations can be combined with geochronological, geomorphological, seismological, and geodetic data into a coherent model of the AD 365 earthquake that is consistent with the historical record [10]. Evidence of tsunamigenic potential for the other parts of the Hellenic plate boundary is patchy, so in this paper we use Western Crete as the Rosetta Stone through which the incomplete evidence from other parts of the Hellenic plate boundary may be interpreted.

The 'sea marks' around the shore of western Crete were first described by Capt. Thomas Spratt [54] who, during a hydrological survey of Crete, identified features formed at or below sea level that had been raised up to 10 metres above sea level in historical time. These features include bio-erosional notches, algal

encrustations, and other remains of marine species that are found in life position [9,53]. Their highest level is often marked by a prominent algal encrustation that is not seen elsewhere on the cliffs below, except where similar constructions are found growing at present sea level [10]. In what follows we shall, for brevity, refer to the uppermost levels of these marine features as palæoshorelines. To our knowledge, in all places where such a palæoshoreline is found, this level also marks a clear transition between (above) rock that has experienced long-lived sub-aerial erosion and (below) submarine erosion or marine encrustation. The palæoshorelines are therefore interpreted as having been formed during the interval between the stabilisation of sea level, ∼6,000 years before present (6 kybp), and the events that lifted them.

Before the recent advances in radiocarbon dating, which allowed the determination of high-precision ages from small samples, the timing of the uplift events was uncertain; indeed the radiometric dates allowed the possibility that the palæoshorelines were uplifted in a series of small events (*e.g.* [9,15,53,55]). Recent high-precision radiocarbon dates from corals preserved between present sea level and the palæoshorelines in Western Crete show, however, that at least 75%, and probably more than 90%, of the post-6-kybp uplift took place in a single event which was contemporaneous, within the uncertainty of radiocarbon dating, with the AD 365 earthquake [10].

The elevations of the palæoshorelines in Western Crete die off smoothly with distance measured north-eastward from the south-west corner of Crete, and this distribution of uplift (observations of *Pirazzoli et al.*, 1996 [9] and *Shaw et al.* [10], Figure 4) is consistent with slip of about 20 m on a fault that dips at about 30° and crops out at the Hellenic Trench [10]. The along-strike length of the fault break is constrained by the absence of uplifted shorelines on Kythera and Gavdos (Figure 4) to be about 100 km [10]. *Shaw et al.* [10] assumed that the fault slipped from the surface to a depth of 45 km, and from their fault parameters they arrived at an estimated magnitude of $M_w = 8.3 - 8.5$. Independently, *Papadimitriou and Karakostas* [8] inferred the parameters of the AD 365 earthquake using the smaller data set of *Pirazzoli et al.*, 1996 [9]. They found a fault of length 160 km dipping at 30° to a depth of 50 km and, imposing a moment of $M_w = 8.3$, solved for a distribution of slip on the fault plane (Figure 4). The observations of uplift can also be fit by slip on a fault that strikes at an angle of ∼ 30° to the Hellenic Trench and dips at about 40° to a depth of 70 km [12].

Although range of fault parameters is consistent with the observations of uplift and with the strike of the major bathymetric features of the region, the uplift is inconsistent with slip on the plate interface (see Figure 1 of Supplementary Material of [10]). In our tsunami simulations (Figure 6) we use the sources of *Shaw et al.* [10] and *Papadimitriou and Karakostas* [8] to investigate the impacts of uncertainties in source size. We do not illustrate the source suggested by [12], which cuts across the principal bathymetric features of the region and seems unlikely to correspond to an active fault.

(c) Evidence from other parts of the plate boundary zone

Rhodes

The eastern coast of Rhodes exhibits a set of palæoshorelines that share many characteristics with those uplifted in Western Crete in AD 365 [14,15]. Their maximum elevations are, however, lower than 4 m and their distribution has been disturbed by relative vertical motions across normal faults that are both perpendicular to [15] and parallel to [13] the uplifted shorelines. The event that lifted up the shorelines is estimated, from the ^{14}C ages of lithophagid shells found between the palæoshorelines and modern sea level, to have occurred in the interval 1600–1100 BC [13]. The youngest ^{14}C age from the lithophagids yields a 2-σ range of 3950–3450 BP (2000-1500 BC) but this range may place the date of the earthquake up to 400 years too early, because lithophagids appear to incorporate small amounts of older carbon from their substrate into their shells [57]. The uplift of the shorelines has also been attributed, on the basis of an uplifted slipway, to the famous earthquake of *c*227 BC that destroyed the Colossus of Rhodes [16].

The morphological similarities between the ∼ 6 kybp palæoshorelines in Rhodes and Western Crete strongly suggest that, as in Crete, the uplift in Rhodes took place in a single event. For our present purpose, it is unimportant whether that uplift was in the 3rd century BC [16] or in late Bronze-Age time [13]. Some of the lithophagids whose ^{14}C dates place uplift in the Bronze Age were collected within about 1 m of present sea level; it therefore seems likely that, whatever the age of the main uplift, the AD 1303 and AD 1481 earthquakes caused negligible subsequent uplift of the shorelines.

Eastern Crete

Although there is widespread evidence of uplift of the shores of Eastern Crete, we are not aware of any palæoshoreline, such as those in Rhodes and Western Crete, that would suggest uplift by a single seismic event. We should not, however, expect significant coastal uplift associated with large or great earthquakes in this part of the plate boundary, because the coast lies close to the maximum down-dip extent of slip on likely fault sources (Figure 4). The observed uplift may result from the uplift of footwalls of the arc-parallel and arc-perpendicular normal faults of the region, though there may also be a regional component to the uplift arising from reverse faulting (*e.g.* [19,59,60]).

The tsunami that affected Alexandria in 1303 was probably generated by an earthquake near Eastern Crete [6,61]. The ground shaking associated with the AD 1303 earthquake seems to have been concentrated in Eastern Crete, though the incompleteness of the historical record means that significant shaking in Rhodes cannot be ruled out [6]. In addition, archæological evidence of widespread earthquake destruction in important Bronze-Age sites [56] suggests that a large or great earthquake occurred near Eastern Crete during the period referred to as Late Minoan IA (LMIA). It has been suggested (*e.g.* [62]) that each site was destroyed by a moderate (magnitude ~ 6) earthquake on a nearby fault. Although the absolute age of LMIA is a perennial matter of dispute between those who accept dates based on radiocarbon and those who do not, the duration of LMIA is agreed to have been about 100 years [58]. Thus the suggestion of multiple moderate earthquakes [62] requires at least 20 magnitude ~ 6 earthquakes on the island within about 100 years. This seems implausible: for comparison, Figure 1a shows that no earthquake of magnitude 5.8 or greater was reported beneath Eastern Crete between 1900 and 2010.

For our tsunami simulations, we place sources along the Pliny Trench, whose expression, near Eastern Crete, is much more pronounced than that of the Strabo Trench (Figures 2 and 4). It seems likely that the other bathymetric low in the region, the Ptolemy Trench, represents an extensional graben within the accretionary prism [19,42]. *Gallen et al.* [42] suggest that extensional faulting in the Ptolemy Trench rules out contractional faulting, and its associated earthquake and tsunami hazards, along the south coast of Crete. They draw this inference on the basis that a north-dipping reverse fault cannot crop out adjacent to the south-dipping normal faults near the southern coast of Crete (Figure 7 of [42]); this argument is irrelevant to the reverse faulting that we discuss here, which crops out far offshore. The bathymetric map (Figure 4), and topographic profiles G and H (Figure 2), suggest that the Pliny and Ptolemy trenches are an example of the well-understood phenomenon of parallel reverse and normal faulting, with the normal faulting being within crust of greater surface elevation and higher gravitational potential energy (*e.g.* [63]; see also [64]).

We consider the Pliny Trench to be the most probable source of a tsunamigenic earthquake in this region but we do not rule out the possibility of large earthquakes on the Strabo and Ptolemy Trenches, showing calculations for these sources in the Supplementary Material.

Peloponnese and Karpathos segments

Evidence for tsunamigenic potential of other parts of the plate boundary is, at present, scarce. The historical record shows two tsunamis associated with earthquakes near the Peloponnese (28th February AD 1629, Kithyra; 22nd January, AD 1899, Kyparissia [6,7]), and uplifted notches on the Strophades Islets (SI in Figure 5a) suggest a large earthquake there about 1,500 years ago [65]. The morphological evidence for late-Quaternary uplift of the coast of the Peloponnese [66] suggests that thrusting in this region may be lifting the surface in a fashion analogous to that of Western Crete [10]. In the section of the boundary between Eastern Crete and Rhodes, which we refer to as the Karpathos segment, the Pliny and Strabo Trenches lie far enough offshore for it to be unlikely that uplift caused even by large earthquakes would be preserved.

Clearly, these observations alone would not justify an insistence that these sections of the plate boundary generate large or great earthquakes. We suggest, however, that in view of their morphological similarities with other parts of the plate boundary that do generate such earthquakes, it would be unwise to assume that the Peloponnese and Karpathos segments do not generate tsunamigenic earthquakes. Accordingly, we carry out tsunami simulations for the model sources shown in Figure 5. Tsunami simulations for alternative choices of source in these regions are shown in the Supplementary Material.

4. Tsunami simulations

We carried out calculations for the tsunamis generated by slip on the fault segments that are illustrated in Figures 4 and 5, and listed in Table 1; calculations for alternative sources are shown in the Supplementary Material. The initial condition for each tsunami simulation is given by a static displacement of the sea floor that is calculated assuming uniform slip of a dislocation in an elastic half-space, using the method of [67] with the relevant source parameters (Table 1). The propagation of the tsunami is calculated using the method of splitting algorithm (MOST, *e.g.* [68–70]). This method solves the depth-integrated non-linear shallow water equation by a finite-difference algorithm that splits the equation, in two spatial dimensions plus time, into a pair of equations in one dimension plus time [70]. MOST has been extensively validated through the hydrodynamic community's standards [69]. Calculation of the details of inundation or run-up are heavily dependent upon detailed bathymetric models for the near-shore environment which, except in a few locations, are not available to us. For this reason, the hydrodynamical simulations stop at the 30-m isobath.

Table 1. The parameters of sources used in the tsunami simulations. The longitudes and latitudes of the intersection of the fault with the surface are given. In each case, slip on the fault is assumed to be in the pure reverse sense (rake=90°) and the fault has uniform slip from the surface to the depth shown.

	Endpoints				Dip	Slip	Depth	
Source	°E	°N	°E	°N		(m)	(km)	Fig.
1. West Crete [10]	23.90	34.80	23.11	35.45	30°	20	45	6a
2. West Crete [8]	24.10	34.57	22.79	35.61	35°	20	45	6b
3. Peloponnese (north)	21.65	36.50	20.40	37.70	30°	20	45	7a
4. Peloponnese (south)	22.60	35.70	21.65	36.50	30°	20	45	7b
5. East Crete (west)	25.70	34.30	24.80	34.10	30°	20	45	8a
6. East Crete (east)	26.85	34.80	25.70	34.30	30°	20	45	8b
7. Karpathos	28.20	35.00	27.30	34.50	30°	20	45	9a
8. Rhodes [13]	28.73	36.61	28.38	36.00	35°	9	40	9b

The lengths of the fault segments that we use are mostly ∼100 km (Table 1), in contrast to the lengths of 200 km or more that have been considered in earlier tsunami scenarios for the Eastern Mediterranean (*e.g.* [1,2,4,5]). The Hellenic Trench is approximately linear for about 400 km, while the Pliny Trench extends for over 200 km. It might, therefore, seem reasonable to postulate that the largest feasible tsunamigenic earthquakes would break the entire lengths of these faults. Indeed we cannot rule out this possibility, but we concentrate here on potential earthquake sources that are no longer than the 100–150 km derived from analysis of the uplifted shorelines of Western Crete and Rhodes [8,10,13,53]. Fault segments of such a length are supported by two further observations. First, changes of 5–10° in the strike of the trenches occur at this scale (see Figures 4 and 5). Secondly, the crust of the Aegean, which overlies the reverse faults that crop out at the Trenches, is broken up by pervasive arc-parallel extensional faulting [19,27]. It seems likely that these faults represent weakness against which rupture may terminate, as observed by Oldham [71] in the great 1897 Assam earthquake, which had similar rupture parameters to the AD 365 earthquake [10,72]. Indeed, *Papadimitriou and Karakostas* [8] assume that such segmentation governed the extent of the AD 365 rupture.

For Source 8, near Rhodes, we adopt the parameters given by [13] (Table 1); for the remaining sources, we assume that slip takes place from the surface to a depth of 45 km. This assumption is supported by the analysis of *Shaw et al.* [10] for the AD 365 earthquake, and by the observation that hypocentres of micro-earthquakes within the overriding plate are shallower than ∼45 km [73,74]. This depth is also the maximum extent of shallowly dipping thrust faulting on the subduction interface [20], as is common in subduction zones [75]. We adopt a uniform slip of 20 m, as estimated for the AD 365 earthquake. Although the lengths of the fault segments are of order 100 km, and therefore the ratio of slip to length that we assume is higher than generally observed in earthquakes (*e.g.* [76]), comparable ratios have been deduced for the

high-slip patches of the 2004, Sumatra and 2011, Tohoku tsunamigenic earthquakes, and for the great 1897 Assam earthquake (*e.g.* [72,77–79]).

In Figures 6 to 9 we illustrate maximum wave heights generated by these sources; we also calculate, for each longitude around the northern shore of Africa and each latitude along the eastern shore of the Mediterranean, the wave height at the location where the water depth shallows to 50 m, showing those calculations as bordering panels in Figures 6 to 9.

Although there is uncertainty in the assumed lengths of, and slips on, the fault segments, this uncertainty is to some extent mitigated by the recognition that our calculations may, with caveats, be re-scaled to take account of different magnitudes of slip and to deal with different lengths of fault segment. In the open ocean, tsunamis propagate in a linear fashion (*e.g.* [80]), and we should expect the wave height to scale linearly with the slip in the earthquake if the other source parameters remain constant. Re-scaling is also possible for sources of different lengths. We illustrate this point by comparing wave heights at the 50-m isobath calculated for the sources of *Shaw et al.* [10] and *Papadimitriou and Karakostas* [8] (Sources 1 and 2, Figure 4, Table 1). These two sources are similar in all their parameters, with the exception that they differ in length by a factor of 1.5, such that the area of sea-floor that is lifted up by Source 2 is 1.5 times greater than for Source 1. Figure 6b shows that the wave heights generated by Source 2 are approximately 1.5 times the height of the waves generated by Source 1. Another example of this scaling is given in Figure S6 of the Supplementary Material, where two candidate sources for a tsunamigenic earthquake near Rhodes, which differ in strike by about 10° and in seismic moment by a factor of 4.5, yield very similar scaled distributions of wave heights.

More generally, the amount of gravitational potential energy put into the water column by slip in an earthquake is proportional to the fault area and to the magnitude of the vertical component of the slip. The product of these two quantities is the scalar moment of the earthquake multiplied by the sine of the dip of the fault and divided by the shear modulus [81]. For earthquake sources in approximately the same region, *i.e.* with approximately the same distributions of water depth, then the amount of energy put into the water column by an earthquake depends only upon its scalar moment and the dip. We should expect small-scale differences between sources to disperse during propagation then, provided that the sources we consider are all long in comparison with the water depth, for fixed fault orientation we should expect wave heights to scale with the moment, as just described.

Clearly, such scaling applies only to sources having the same strike and lying in close proximity to one another. We also emphasise that, because propagation becomes pronouncedly non-linear in shallow water and for inundation of land, our remarks about scaling do not apply to water shallower than the 50-m isobath illustrated in Figures 6 to 9. Accurate analysis of run-up and inundation requires detailed knowledge of local bathymetry and land conditions, which are not available to us.

A significant difference between our study and earlier studies of the propagation of tsunamis from the Hellenic plate boundary arises from our recognition of variation by almost 90° in the strike of potential sources along the boundary. The waves of greatest height propagate, along the relatively short paths between sources and the opposite side of the Mediterranean, in the direction approximately perpendicular to the strike of the source with little lateral spreading. In consequence, the distribution of wave heights along the coast of North Africa differ greatly between sources in Western Crete (Figure 6) and those nearby in the Peloponnese (Figure 7). Even the relatively small difference in strike between the two model source segments beneath Eastern Crete (Figure 4) results in appreciably different distributions of wave height along the coast of Egypt (Figure 8).

Figure 10 shows the maximum wave heights at the 50-m isobath for nine large cities along the coast of North Africa and the Levant, calculated for the eight sources listed in Table 1. All these calculations are for a standard slip (see Table 1). As discussed above, it is not possible to convert these wave heights into accurate estimates of run-up without further detailed calculations employing high-resolution, high-precision maps of near-shore bathymetry. We may, nevertheless, make comparisons among the different sites. Recall that Alexandria and much of the Nile Delta were devastated by the AD 365 tsunami [6,50,51], which was generated by an earthquake similar to Sources 1 and 2. The wave heights offshore from Alexandria calculated from those sources are about 2 m (Figure 10). Wave heights off Benghazi, Derna, and Tobruk exceed 2 metres for all of the sources except Source 8, and the calculated wave heights off Alexandria for

sources 5, 6, and 7, near Eastern Crete and Karpathos (Figures 4 and 5) are also higher than those calculated for the source of AD 365.

The wave heights calculated for Port Said and the Levantine coast are generally lower than 1 m, and any assessment of tsunami hazard in this region must also take account of tsunami sources local to that region [49], which are beyond the scope of this paper.

5. Discussion and Conclusions

Studies of tsunami hazard commonly start with a model that is strongly constrained by the locations of earthquakes that have occurred in the 50 years or so during which worldwide seismic networks have been operating, though such models may be modified by information drawn from fault maps (*e.g.* [1–3,82]). The observations that we summarise here suggest that it would be unwise to treat seismological data as the primary source of information for estimating tsunami hazard in the Eastern Mediterranean. Most of the deformation across the Hellenic plate boundary is aseismic [17], and we are aware of no clear evidence from seismology alone for the existence of the faults that slipped in the tsunamigenic earthquakes of AD 365 or AD 1303.

Here, we have taken an approach that is based on combining geological, geodetic, geomorphological, geochronological, historical and seismological data to form a model of the tsunamigenic potential of the plate boundary (*e.g.* [6,7,10–14,19–21,25,26,33]). The central aspects of this model are that the subduction fault itself slips in a predominantly aseismic fashion, and that the tsunami hazard is associated with more steeply dipping faults within the accretionary prism on top of the Nubian plate, which deliver rare great earthquakes [8,10–12,53]. One of these faults crops out along the prominent bathymetric scarp of the 400-km-long Hellenic Trench. Analysis of uplift in the AD 365 earthquake suggests that, at least beneath Western Crete, this fault dips at $\sim 30^{\circ}$ to a depth of 40–45 km [8,10]. Although this fault bears some resemblance to "splays" that have been associated with actual or potential tsunamis in other subduction zones (*e.g.* [83–86]) it differs from them in that it seems to be the primary seismic and tsunamigenic fault, from the surface to a depth of 40–45 km. The faulting at the eastern end of the Hellenic plate boundary is more uncertain, and perhaps more complicated. Here, the overall relative motion is highly oblique, but the slip vectors of earthquakes near the top of the Nubian plate indicate that slip may be partitioned, with the transcurrent component of motion taking place on the subduction fault while the contractional component is absorbed on one or more faults within the upper plate ([13] and Figures 3, 4, and 5b).

We have carried out simulations of tsunamis generated by candidate earthquake sources around the Hellenic plate boundary (Table 1). In two cases, the sources are constrained by detailed studies: of the AD 365 earthquake in Western Crete [8,10,12], and of the earthquake in Roman or Bronze-Age time near Rhodes [13–16]. In the remaining cases the locations are decided primarily on the basis of geomorphological expressions of faulting. Although there are uncertainties attached to this procedure, the orientation of individual fault segments are well constrained by prominent bathymetric scarps with which they are associated (Figures 4 and 5). For a given orientation of fault segment, the calculated wave heights scale, to a good approximation, with the moment of the causative earthquake (see discussion of Figure 6).

Much attention has been paid recently to the uncertainties involved in calculating run-up and inundation for a given tsunami source. In the Eastern Mediterranean at least, the dominant uncertainties are those associated with the source itself. For any given location on the coast of North Africa, the impact of a tsunami is dependent principally upon the moment of the causative earthquake, and upon where along the Hellenic plate boundary the earthquake occurs (which determines the orientation of the fault, hence the direction in which the greatest energy propagates in the tsunami, compare Figures 6 to 9). We remind the reader that the near-shore wave heights calculated in those figures cannot be translated directly into predictions of run-up, for the reasons discussed in Section 4. A sensible approach is to recognise that the AD 365 and AD 1303 earthquakes caused devastating tsunamis on the coast of Africa and that similarly-sized earthquakes in the future will likely do the same. Our calculations should be taken as showing, for a given location of tsunamigenic earthquake, which locations are likely to suffer more than others.

Finally, we contend that a probabilistic assessment of tsunami hazard in the Eastern Mediterranean would, given the present state of knowledge, be misguided. As we mention above, measurements of seismicity in the Hellenic plate boundary over the past few decades are largely, perhaps totally, irrelevant

to the faults that cause the tsunamis. Although some certainty attaches to the locations of the hazardous faults, the estimates from GPS of the contractional strain that will eventually be released in earthquakes along those faults differ by a factor of ten or more [10,21,87]. Given such uncertainties it is prudent to take a precautionary approach to the hazard.

Acknowledgment

We benefited from many discussions with B. Shaw, T. Higham, N. Kalligeris and the late N. N. Ambraseys. We are grateful to R. Bilham for a helpful review, and for suggesting Figure 10; we also thank an anonymous reviewer for their detailed and thoughtful review. This work was supported by the Natural Environmental Research Council through grant NE/J02001X/1. CES's work was funded by the FP7 program ASTARTE. AH is supported by a Shell Scholarship. Most of the figures were made using the Generic Mapping Tools [88].

References

1. Lorito, S., Tiberti, M. M., Basili, R., Piatanesi, A. & Valensise, G.
Earthquake-generated tsunamis in the Mediterranean sea: Scenarios of potential threats to southern Italy.
J. Geophys. Res. **113**, 14 (2008).
2. Tinti, S., Armigliato, A., Pagnoni, G. & Zaniboni, F.
Scenarios of giant tsunamis of tectonic origin in the Mediterranean.
ISET Journal of Earthquake Technology **42**, 171–188 (2005).
3. Sørensen, M. B., Spada, M., Babeyko, A., Wiemer, S. & Grünthal, G.
Probabilistic tsunami hazard in the Mediterranean Sea.
Journal of Geophysical Research **117**, B01305 (2012).
4. Valle, B. L. *et al.*
Plausible megathrust tsunamis in the Eastern Mediterranean Sea.
Proceedings of the Institution of Civil Engineers **167**, 99–105 (2014).
5. Yolsal, S., Taymaz, T. & Yalçiner
Understanding tsunamis, potential source regions and tsunami-prone mechanisms in the Eastern Mediterranean.
Geol. Soc. Lond. Spec. Pub. **291**, 201–230 (2007).
6. Ambraseys, N. N.
Earthquakes in the Mediterranean and Middle East (Cambridge University Press, 2009).
7. Ambraseys, N. & Synolakis, C.
Tsunami catalogs for the Eastern Mediterranean, revisited.
J. of Earthquake Eng. **14**, 309–330 (2010).
8. Papadimitriou, E. E. & Karakostas, V. G.
Rupture model of the great AD 365 Crete earthquake in the southwestern part of the Hellenic Arc.
Acta Geophys. **56**, 293–312 (2008).
9. Pirazzoli, P. A., Laborel, J. & Stiros, S.
Earthquake clustering in the Eastern Mediterranean during historical times.
J. Geophys. Res. **101**, 6,083–6,098 (1996).
10. Shaw, B. *et al.*
Eastern Mediterranean tectonics and tsunami hazard inferred from the AD 365 earthquake.
Nature Geosci. **1**, 268–276 (2008).
11. Stiros, S.
The AD 365 Crete earthquake and possible seismic clustering during the fourth to sixth centuries AD in the Eastern Mediterranean: a review of historical and archaeological data.
J Struct Geol 545–562 (2001).
12. Stiros, S. C. & Drakos, A.
A fault model for the tsunami-associated, magnitude ≥ 8.5 Eastern Mediterranean, AD 365 earthquake.
Z. Geomorphol. **146,** (2006).
13. Howell, A., Jackson, J., England, P., Higham, T. & Synolakis, C.
Late Holocene uplift of Rhodes, Greece: Evidence for a large tsunamigenic earthquake and the implications for the tectonics of the eastern Hellenic Trench system.

Geophys. J. Int. In Press (2015).

14. Kontogianni, V., Tsoulos, N. & Stiros, S.
Coastal uplift, earthquakes and active faulting of Rhodes Island (Aegean Arc): modeling based on geodetic inversion.
Marine Geology **186**, 299–317 (2002).
15. Pirazzoli, P. *et al.*
Crustal block movements from Holocene shorelines: Rhodes island (Greece).
Tectonophysics **170**, 89–114 (1989).
16. Stiros, S. & Blackman, D. J.
Seismic coastal uplift and subsidence in Rhodes island, Aegean arc: evidence from an uplifted ancient harbour.
Tectonophysics 1–31 (2013).
17. Jackson, J. & M^{c}Kenzie, D. P.
The relationship between plate motions and seismic moment tensors and the rate of active deformation in the Mediterranean and Middle East.
Geophys. J. R. Astr. Soc. **93**, 45–73 (1988).
18. Benetatos, C., Kiratzi, A., Papazachos, C. & Karakaisis, G.
Focal mechanisms of shallow and intermediate depth earthquakes along the Hellenic Arc.
J. Geodyn. **37**, 253–296 (2004).
19. Caputo, R. *et al.*
Active faulting on the island of Crete (Greece).
Geophysical Journal International **183**, 111–126 (2010).
20. Shaw, B. & Jackson, J.
Earthquake mechanisms and active tectonics of the Hellenic subduction zone.
Geophysical Journal International **181**, 966–984 (2010).
21. Vernant, P., Reilinger, R. & M^{c}Clusky, S.
Geodetic evidence for low coupling on the Hellenic subduction plate interface.
Earth Planet. Sci. Lett. **385**, 122–129 (2014).
22. Nocquet, J.-M.
Present-day kinematics of the Mediterranean: A comprehensive overview of GPS results.
Tectonophysics 1–23 (2012).
23. Reilinger, R. *et al.*
GPS constraints on continental deformation in the Africa-Arabia-Eurasia continental collision zone and implications for the dynamics of plate interactions.
J. Geophys. Res. **111** (2006).
24. Aktuğ, B. *et al.*
Deformation of western Turkey from a combination of permanent and campaign GPS data: Limits to block-like behavior.
J. Geophys. Research **114**, 1–22 (2009).
25. Floyd, M. A. *et al.*
A new velocity field for Greece: Implications for the kinematics and dynamics of the Aegean.
J. Geophys. Res. **115**, B10403 (2010).
26. Jackson, J.
Active tectonics of the Aegean region.
Ann. Rev. Earth Planet. Sci. **22**, 239–271 (1994).
27. Armijo, R., Lyon-Caen, H. & Papanastassiou, D.
East–west extension and Holocene normal–fault scarps in the Hellenic arc.
Geology **20**, 491–494 (1992).
28. Huchon, P., Lybéris, N., Angelier, J., Pichon, X. L. & Renard, V.
Tectonics of the Hellenic Trench: a synthesis of Sea-Beam and submersible observations.
Tectonophysics **86**, 69–112 (1982).
29. Kiratzi, A.
The January 2012 earthquake sequence in the Cretan Basin, south of the Hellenic volcanic arc: Focal mechanisms, rupture directivity and slip models.
Tectonophysics **586**, 160–172 (2013).
30. Engdahl, E., van der Hilst, R. & Buland, R.
Global teleseismic earthquake relocation with improved travel times and procedures for depth determination.
Bull. Seismol. Soc. Amer. **88**, 722–743 (1998).

31. International Seismological Centre.
EHB Bulletin.
Int. Seis. Cent., Thatcham, United Kingdom (2011).
http://www.isc.ac.uk.
32. Engdahl, E. R. & Villaseñor, A.
Global seismicity: 1900–1999.
In Lee, W. H. K., Jennings, P., Kanamori, H. & Kisslinger, C. (eds.) *IASPEI Handbook of Earthquake and Engineering Seismology, Part A*, 665–690 (Academic Press, Boston, 2002).
33. Ambraseys, N. & Jackson, J. A.
Faulting associated with historical and recent earthquakes in the Eastern Mediterranean region.
Geophys. J. Int. **133**, 390–406 (1998).
34. Taymaz, T., Jackson, J. & M^{c}Kenzie, D.
Active tectonics of the north and central Aegean Sea.
Geophys. J. Int. **106**, 433–490 (1991).
35. Chaumillon, E. & Mascle, J.
From foreland to forearc domains: new multichannel seismic reflection survey of the Mediterranean ridge accretionary complex (Eastern Mediterranean).
Marine Geology **138**, 237–259 (1997).
36. Huguen, C. *et al.*
Deformational styles of the eastern Mediterranean Ridge and surroundings from combined swath mapping and seismic reflection profiling.
Tectonophysics **343**, 21–47 (2001).
37. Mascle, J. & Chaumillon, E.
An overview of Mediterranean Ridge collisional accretionary complex as deduced from multichannel seismic data.
Geo-Mar. Lett. **18**, 81–89 (1998).
38. Le Pichon, X. & Angelier, J.
The Hellenic Trench system: a key to the neotectonic evolution of the Eastern Mediterranean area.
Tectonophysics **60**, 1–42 (1979).
39. Kreemer, C. & Chamot-Rooke, N.
Contemporary kinematics of the southern Aegean and the Mediterranean Ridge.
Geophys J Int **157**, 1377–1392 (2004).
40. Mascle, J., Cleac'h, A. & Jongsma, D.
The eastern Hellenic margin from Crete to Rhodes: example of progressive collision.
Marine Geology **73**, 145–168 (1986).
41. M^{c}Kenzie, D.
Active tectonics of the Alpine-Himalayan belt – Aegean sea and surrounding regions.
Geophys. J. Royal Astron. Soc. **55**, 217–254 (1978).
42. Gallen, S. F. *et al.*
Active simultaneous uplift and margin-normal extension in a forearc high, Crete, Greece.
Earth Planet. Sci. Lett. **398**, 11–24 (2014).
43. Mascle, J. *et al.*
The Hellenic margin from eastern Crete to Rhodes: preliminary results.
Tectonophysics **86**, 133–147 (1982).
44. Özbakır, A. D., Şengör, A. M. C., Wortel, M. J. R. & Govers, R.
The Pliny–Strabo trench region – a large shear zone resulting from slab tearing.
Earth and Planetary Science Letters **375**, 188–195 (2013).
45. Jongsma, D.
Bathymetry and shallow structure of the Pliny and Strabo Trenches, south of the Hellenic Arc.
Geological Society of America Bulletin **88**, 797–805 (1977).
46. Peters, J. & Huson, W.
The Pliny and Strabo trenches (eastern Mediterranean): Integration of seismic reflection data and SeaBeam bathymetric maps.
Marine Geology **64**, 1–17 (1985).
47. ten Veen, J. H., Boulton, S. J. & Alçiçek, M. C.
From palaeotectonics to neotectonics in the Neotethys realm: The importance of kinematic decoupling and inherited structural grain in SW Anatolia (Turkey).
Tectonophysics **473**, 261–281 (2009).

48. Taymaz, T., Jackson, J. & Westaway, R.
Earthquake mechanisms in the Hellenic Trench near Crete.
Geophys. J. Int. **102**, 695–731 (1990).
49. Salamon, A., Rockwell, T., Ward, S. N., Guidoboni, E. & Comastri, A.
Tsunami hazard evaluation of the eastern Mediterranean: Historical analysis and selected modeling.
Bulletin of the Seismological Society of America **97**, 705–724 (2007).
50. Ambraseys, N., Melville, C. & Adams, R. D.
The Seismicity of Egypt, Arabia and the Red Sea: A historical review (Cambridge University Press, Cambridge, 1994).
51. Guidoboni, E., Comastri, A. & Traina, G.
Catalogue of Ancient Earthquakes in the Mediterranean Area up to the 10th Century (Istituto Nazionale di Geofisica, Bologna, Italy, 1994).
52. Pirazzoli, P.
The Early Byzantine tectonic paroxysm.
Zeitschr. Geomorph. (Suppl.) **62**, 31–49 (1986).
53. Pirazzoli, P. A., Thommeret, J., Thommeret, Y., Laborel, J. & Montaggioni, L. F.
Crustal block movements from Holocene shorelines: Crete and Antikithera.
Tectonophysics **86**, 27–43 (1982).
54. Spratt, T. A. B.
Travels and Researches in Crete Vol. 2 (J. van Voorst, London, 1865).
55. Pirazzoli, P. A., Laborel, J. & Stiros, S.
Coastal indicators of rapid uplift and subsidence: Examples from Crete and other Eastern Mediterranean sites.
Zeitscrift für Geomorphologie Suppl. **102**, 21–35 (1996).
56. Driessen, J. & Macdonald, C. F.
The troubled island. Minoan Crete before and after the Santorini eruption.
Aegaeum **17** (1997).
57. Shaw, B., Jackson, J. A., Higham, T. F. G., England, P. C. & Thomas, A. L.
Radiometric dates of uplifted marine fauna in Greece: Implications for the interpretation of recent earthquake and tectonic histories using lithophagid dates.
Earth Planet Sc Lett 1–10 (2010).
58. Manning, S. *et al.*
Chronology for the Aegean Late Bronze Age 1700-1400 BC.
Science **312**, 565–569 (2006).
59. Gaki-Papanastassiou, K., Karymbalis, E., Papanastassiou, D. & Maroukian, H.
Quaternary marine terraces as indicators of neotectonic activity of the Ierapetra normal fault SE Crete (Greece).
Geomorphology **104**, 38–46 (2009).
60. Peters, J. M., Troelstra, S. R. & van Harten, D.
Late Meogene and Quaternary vertical movements in eastern Crete and their regional significance.
J. Geol. Soc. Lond. **142**, 501–513 (1985).
61. Guidoboni, E. & Comastri, A.
The large earthquake of 8 August 1303 in Crete: seismic scenario and tsunami in the Mediterranean area.
J. Seismology **1**, 55–72 (1997).
62. Monaco, C. & Tortorici, L.
Faulting and effects of earthquakes on Minoan archaeological sites in Crete (Greece).
Tectonophysics **382**, 103–116 (2004).
63. Dalmayrac, B. & Molnar, P.
Parallel thrust and normal faulting in Peru and constraints on the state of stress.
Earth Planet. Sci. Lett. **55**, 473–481 (1981).
64. Farías, M., Comte, D., Roecker, S., Carrizo, D. & Pardo, M.
Crustal extensional faulting triggered by the 2010 Chilean earthquake: The Pichilemu seismic sequence.
Tectonics **30**,TC6010 (2011).
65. Stiros, S. C., Pirazzoli, P. A. & Fontugne, M.
New evidence of Holocene coastal uplift in the Strophades Islets (W Hellenic Arc, Greece).
Mar Geol **267**, 207–211 (2009).
66. Kelletat, D., Kowalczyk, G., Schröder, B. & Winter, K.

A synoptic view of the neotectonic development of the Peloponnesian coastal regions.
Zetscrift der Deutsche Geologische Gesellschaft **27**, 447–465 (1976).

67. Okada, Y.
Internal deformation due to shear and tensile faults in a half-space.
Bull. Seismol. Soc. Amer. **82**, 1018 (1992).
68. Flouri, E. T., Kalligeris, N., Alexandrakis, G., Kampanis, N. A. & Synolakis, C. E.
Application of a finite difference computational model to the simulation of earthquake generated tsunamis.
Applied Numerical Mathematics **67**, 111–125 (2013).
69. Synolakis, C. E., Bernard, E. N., Titov, V. V., Kânoğlu, U. & González, F. I.
Validation and verification of tsunami numerical models.
Pure appl. geophys. **165**, 2197–2228 (2008).
70. Titov, V. & Synolakis, C.
Numerical modeling of tidal wave runup.
Journal of Waterway, Port, Coastal, and Ocean Engineering **124**, 157–171 (1998).
71. Oldham, R. D.
Report on the great earthquake of 12th June 1897.
Memoirs of the Geological Survey of India **29**, 1–379 (1899).
72. Bilham, R. & England, P.
Plateau 'pop-up' in the great 1897 Assam earthquake.
Nature **410**, 806–9 (2001).
73. De Chabalier, J. *et al.*
A detailed analysis of microearthquakes in western Crete from digital three-component seismograms.
Geophysical Journal International **110**, 347–360 (1992).
74. Meier, T., Rische, M., Endrun, B., Vafdis, A. & Harjes, H.-P.
Seismicity of the Hellenic subduction zone in the area of western and central Crete observed by temporary local seismic networks.
Tectonophysics **383**, 149–169 (2004).
75. Tichelaar, B. W. & Ruff, L.
Depth of seismic coupling along subduction zones.
J. Geophys. Res. **98**, 2107–2037 (1993).
76. Wells, D. & Coppersmith, K.
New empirical relationships among magnitude, rupture length, rupture width, rupture area, and surface displacement.
Bull. Seismol. Soc. Amer. **84**, 974–1002 (1994).
77. Koketsu, K. *et al.*
A unified source model for the 2011 Tohoku earthquake.
Earth and Planetary Science Letters **310**, 480–487 (2011).
78. Subarya, C. *et al.*
Plate-boundary deformation associated with the great Sumatra–Andaman earthquake.
Nature **440**, 46–51 (2006).
79. Yue, H. & Lay, T.
Source rupture models for the Mw 9.0 2011 Tohoku earthquake from joint inversions of high-rate geodetic and seismic data.
B Seismol Soc Am **103**, 1242–1255 (2013).
80. Synolakis, C. & Bernard, E.
Tsunami science before and beyond Boxing Day 2004.
Phil. Trans. Royal Soc. Lond., A **364**, 2231–2265 (2006).
81. Aki, K. & Richards, P. G.
Quantitative Seismology (University Science Books, Sausalito, California, 2002), second edn.
82. Basili, R. *et al.*
Integrating geologic fault data into tsunami hazard studies.
Nat. Hazards Earth Syst. Sci. **13**, 1025–1050 (2013).
83. Chapman, J. B., Elliott, J., Doser, D. I. & Pavlis, T. L.
Slip on the Suckling Hills splay fault during the 1964 Alaska earthquake.
Tectonophysics **637**, 191–197 (2014).
84. Moore, G. F. *et al.*
Three-dimensional splay fault geometry and implications for tsunami generation.
Science **318**, 1128–1131 (2007).

627 85. Park, J., Tsuru, T., Kodaira, S., Cummins, P. & Kaneda, Y.
628 Splay fault branching along the Nankai subduction zone.
629 *Science* **297**, 1157–1160 (2002).
630 86. Strasser, M. *et al.*
631 Origin and evolution of a splay fault in the Nankai accretionary wedge.
632 *Nature Geoscience* **2**, 648–652 (2009).
633 87. Ganas, A. & Parsons, T.
634 Three-dimensional model of Hellenic Arc deformation and origin of the Cretan uplift.
635 *J. Geophys. Research* **114**, 1–14 (2009).
636 88. Wessel, P. & Smith, W. H. F.
637 Generic Mapping Tools: Improved version released.
638 *EOS Trans. Amer. Geophys. U.* **94**, 409–410 (2013).

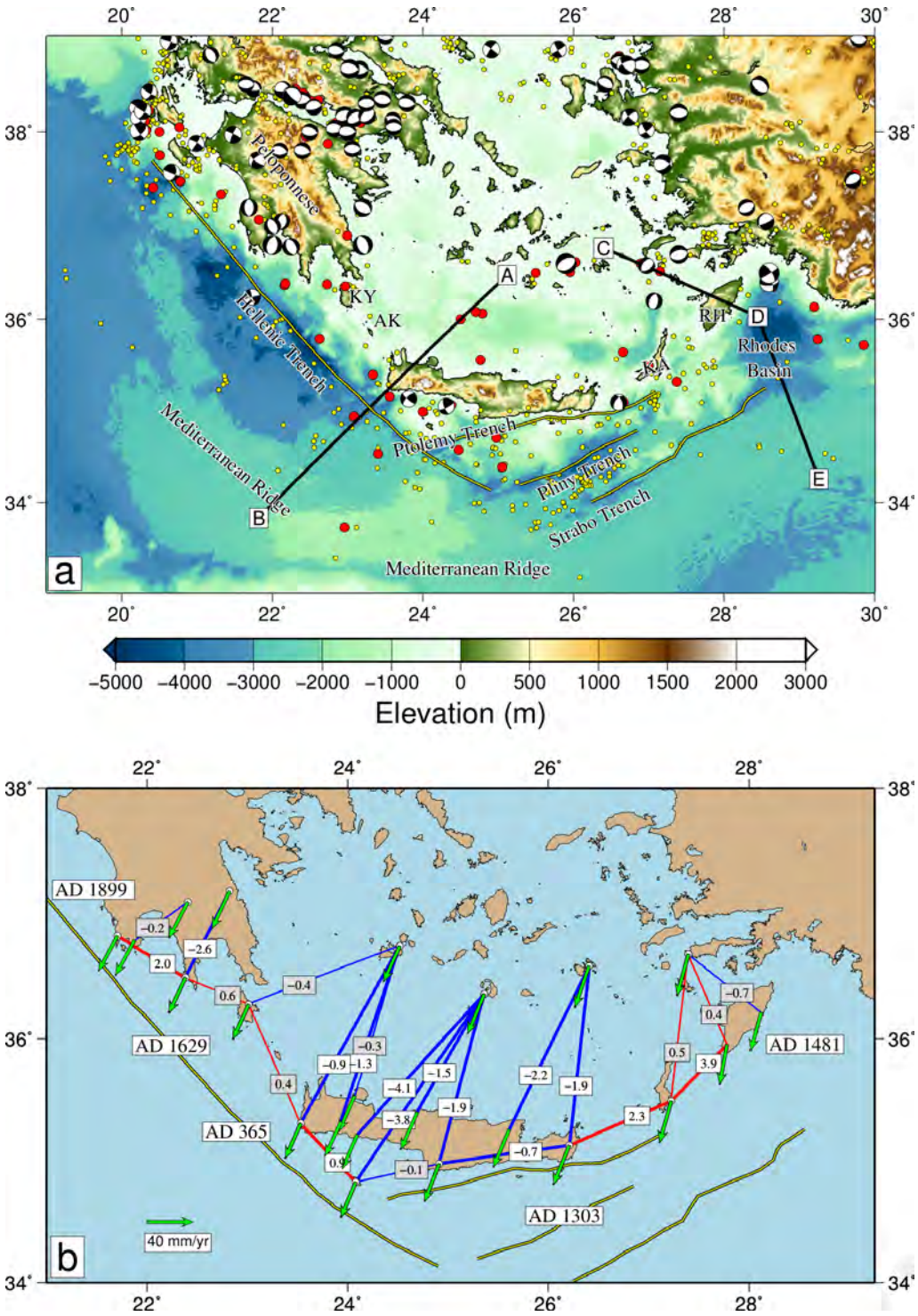

Figure 1. The Hellenic plate boundary zone. a) Topography (colour scale at the bottom) and locations discussed in the text. Abbreviations: **A**nti**K**ythera, **KY**thera, **KA**rpathos, **RH**odes. Dots show the epicentres of shallow (depth $<$30 km) earthquakes for 1960–2010 from the EHB catalogue [30,31] and for 1900–1999 from the catalogue of *Engdahl and Villaseñor* [32]; yellow and red dots show earthquakes with magnitudes, respectively, < 5.8 and ≥ 5.8. Focal mechanisms are of earthquakes within the upper crust of the Eurasian lithosphere [20,33,34]. The lines AB and CDE show the locations of sections in Figure 3. b) Relative motions between the Aegean and Nubia. Green arrows show the velocities of GPS sites in the Peloponnese and the islands of the southern Aegean with respect to the Nubian plate; the velocities of [22] are rotated into the Nubian frame using the pole of [23]. Baselines between GPS sites are shown by red (lengthening) and blue (contracting) lines. Rates of change of length of line (in mm/yr) are shown in boxes. Thicker lines and white boxes correspond to baselines whose length changes are greater than their 1-σ uncertainties; thinner lines and grey boxes denote length changes that are not resolved at the 1-σ level. Dates (AD 365–AD 1899) refer to approximate source regions of tsunamigenic earthquakes discussed in Section 3.

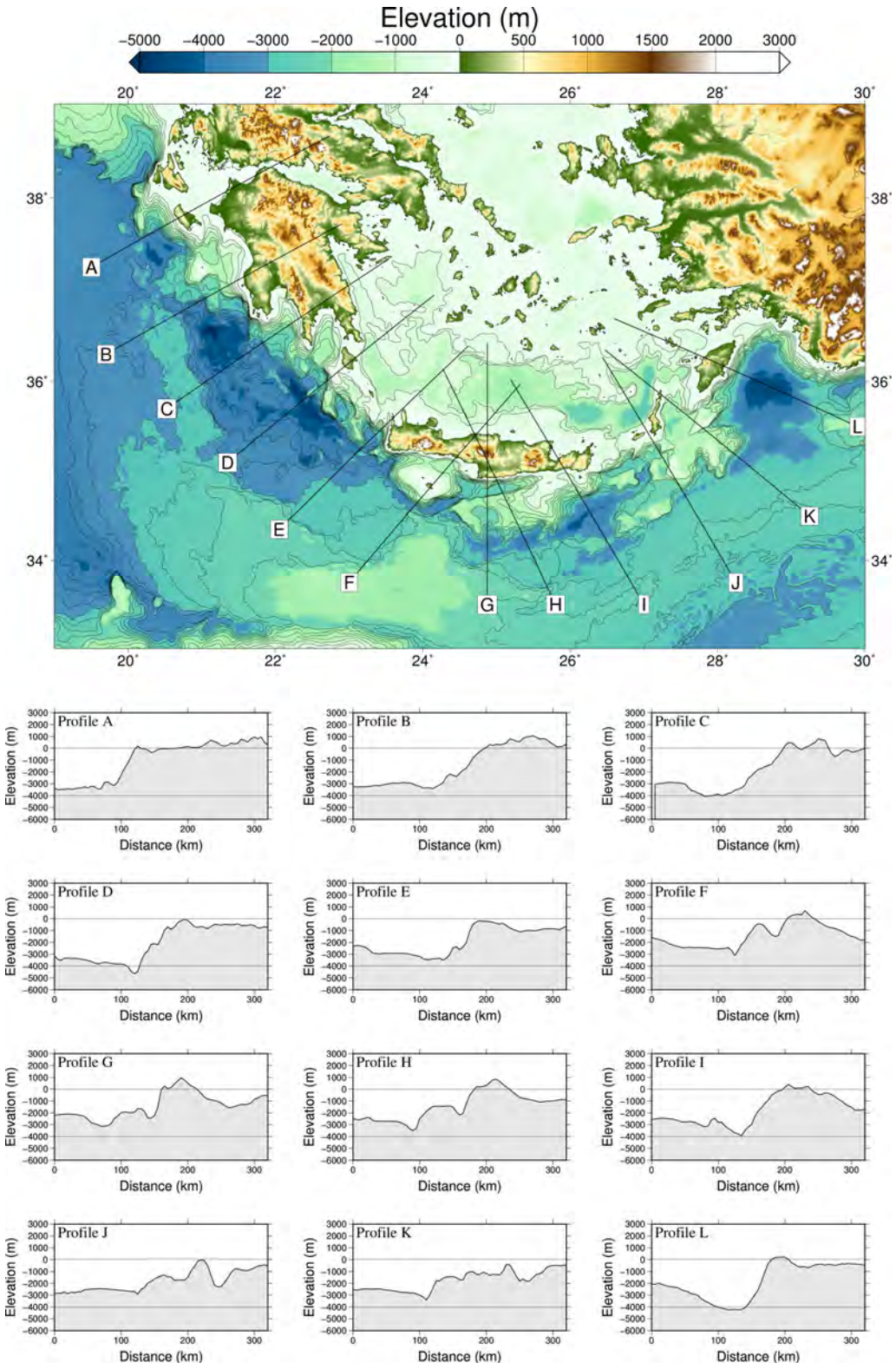

Figure 2. Profiles of bathymetry along twelve sections perpendicular to the Hellenic, Pliny, and Strabo Trenches.

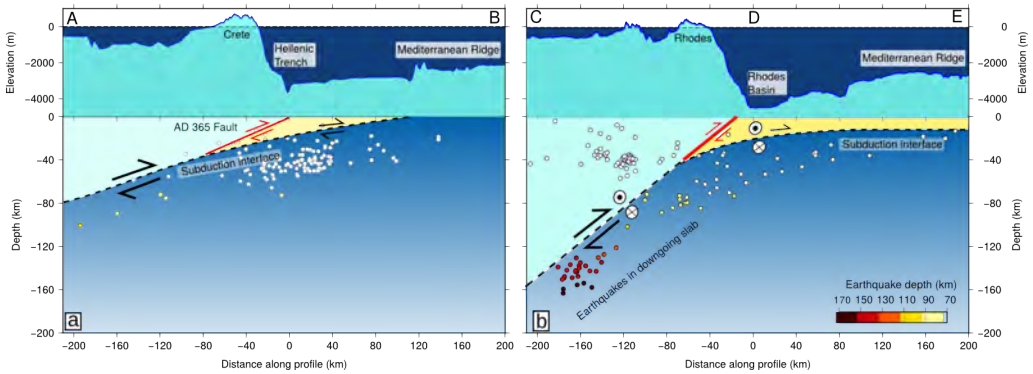

Figure 3. Sketches of the configuration of faulting in the Hellenic plate boundary, after [10,13]. The locations of the sections are shown on Figure 1a. The lithosphere of the south Aegean and its underlying upper mantle are shown to the left of each panel in light blue; Nubian lithosphere and its upper mantle are shown to the right in darker blue. At the top of each panel, topography is shown at an exaggerated scale. Yellow shading represents the thick sedimentary pile on top of the Mediterranean sea floor. The subduction interface is shown by the dashed line separating the Nubian plate from the overlying sediment and the Aegean lithosphere. In each profile, the rate of slip on the subduction boundary decreases towards the surface, leading to contractional strain (seen in the GPS data of Figure 1b) that is released in reverse faulting at the locations shown in red.

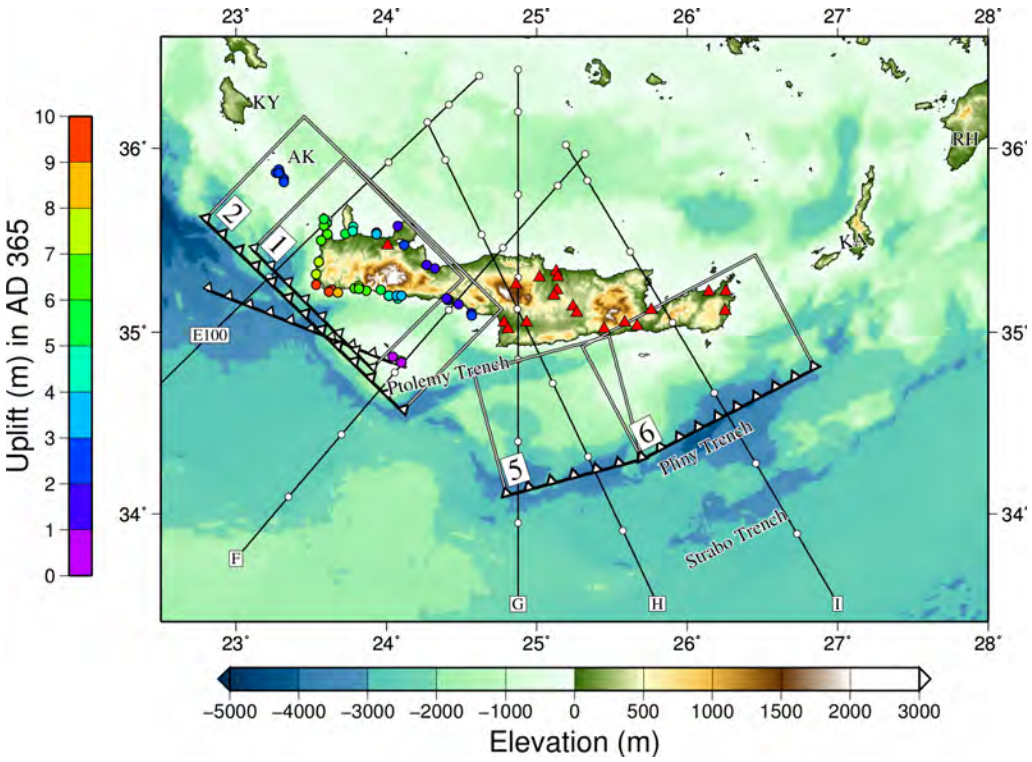

Figure 4. Location map for potential tsunami sources near Crete. Coloured circles (scale to left) show the observed elevations above present sea level of palæoshorelines lifted by the earthquake of AD 365 [9,10]. Rectangles with fault symbols show the projection on the surface of fault sources used in this study: [1] location of AD 365 earthquake inferred by *Shaw et al.* [10]; [2] location of AD 365 earthquake inferred by *Papadimitriou and Karakostas* [8]. Tsunami simulations for these sources are illustrated in Figure 6. Planes [5] and [6] show locations of model sources for the tsunami simulations illustrated in Figure 8. Fault symbol without accompanying rectangle shows the location of the AD 365 event inferred by *Stiros and Drakos* [12]; this plane dips NNE at 40° to a depth of 70 km. Red triangles show the locations of substantial Minoan edifices that suffered earthquake damage in Late Minoan IA time [56]. The lines of Profiles E–I (Figure 2) are decorated with white dots at intervals of 50 km from their southern ends; the label E100 is at 100 km from the southern end of Profile E.

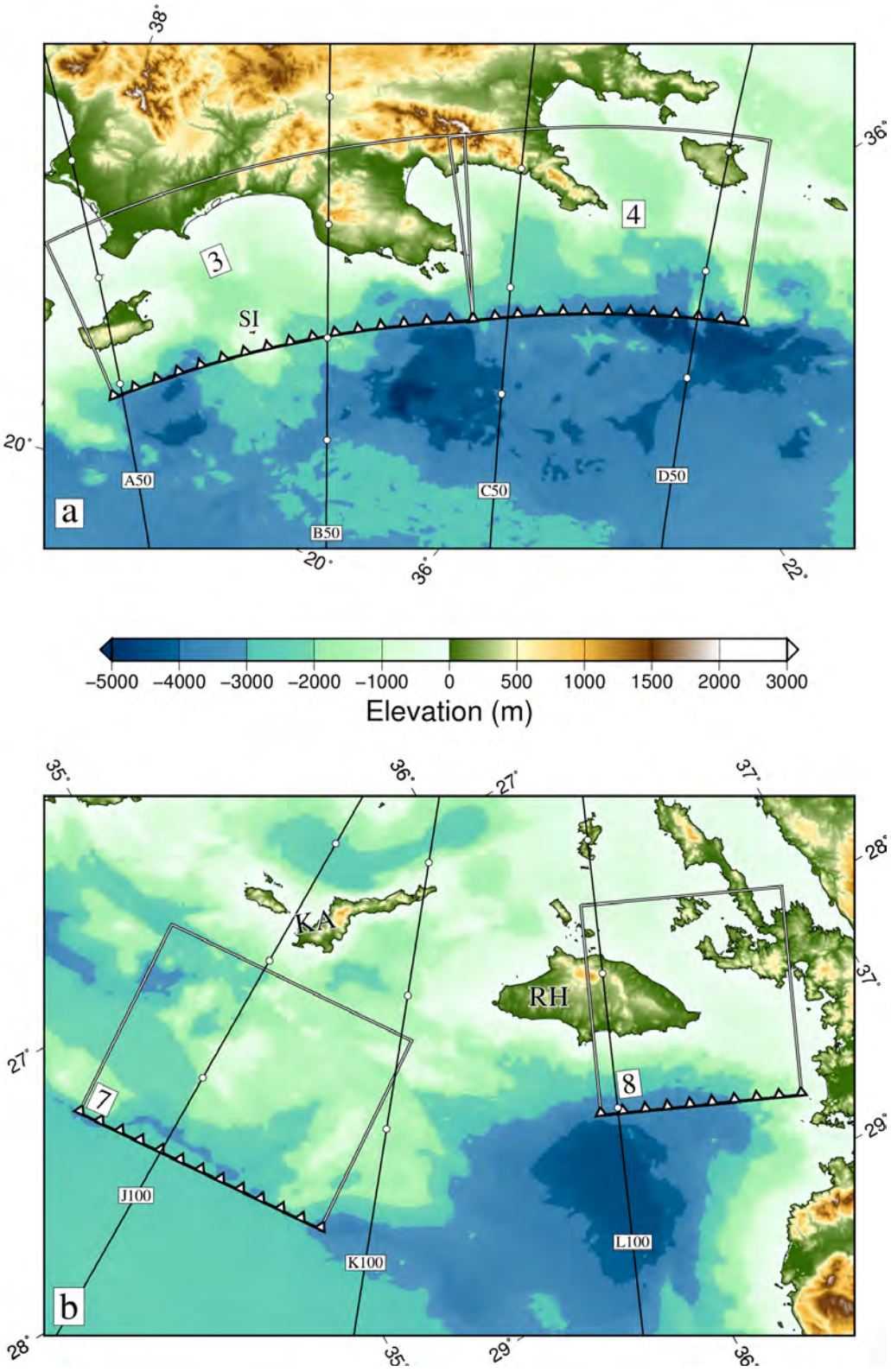

Figure 5. Location map for potential tsunami sources (a) near the Peloponnese and (b) near the eastern end of the Hellenic plate boundary. Symbols as for Figure 4. (a) Rectangles and fault symbols show the locations of the model sources near the Peloponnese; the tsunami simulations are illustrated in Figure 7. The lines of Profiles A–D (Figure 2) are decorated with white dots at intervals of 50 km from their southern ends; the label of each profile is given at 50 km from its southern end. (b) Rectangles show the locations of the model sources near Karpathos and Rhodes (following [13]); the tsunami simulations are illustrated in Figure 9. Numbers refer to sources listed in Table 1. The lines of Profiles K–L (Figure 2) are decorated with white dots at intervals of 50 km from their southern ends; the profiles are labelled at 100 km from their southern ends.

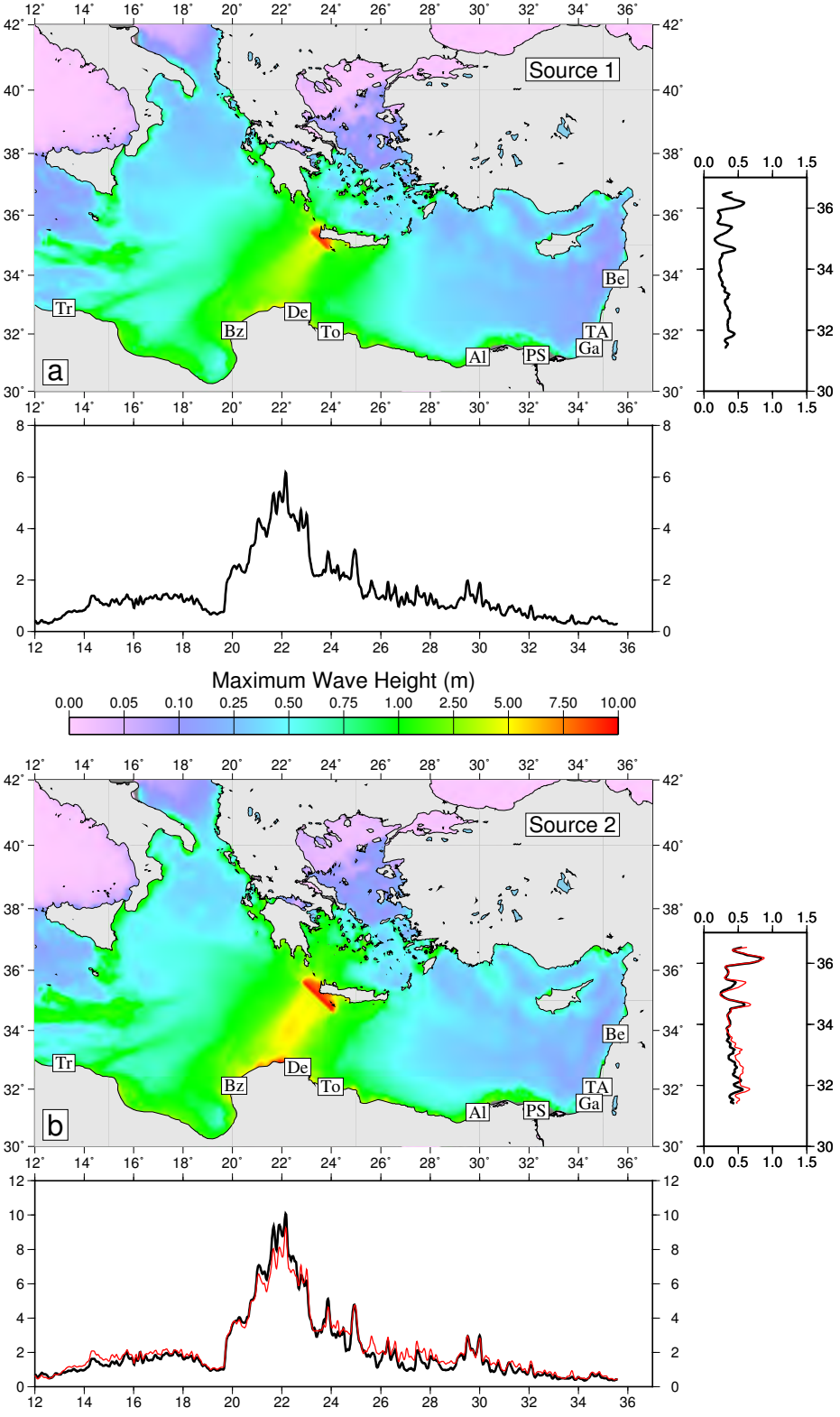

Figure 6. Hydrodynamic calculations of maximum wave heights (above undisturbed sea level) in the Eastern Mediterranean basin and profiles of maximum wave height along near-shore 50-m isobaths. Colours (colour scale in centre) display the maximum height of the sea surface above its undisturbed level in the 4 hours following the uplift of the sea floor that initiates the calculation. Bordering panels show maximum wave height in metres, for that same interval, recorded along the 50-m isobath near the coast of Africa (bottom panel) and the Levant (right-hand panel). In (b) black lines are calculated for Source 2 (Table 1) with 20 m of slip; the red lines represent wave heights calculated from Source 1, also with 20 m of slip, but with their amplitudes multiplied by a factor of 1.5 (which represents the ratio of the seismic moment of the two sources). The locations of cities referred to in Figure 10 are denoted by two-letter abbreviations: **Tr**ipoli; **B**engha**z**i; **De**rna; **To**bruk; **Al**exandria; **P**ort **S**aid; **Ga**za; **T**el **A**viv; **Be**irut.q

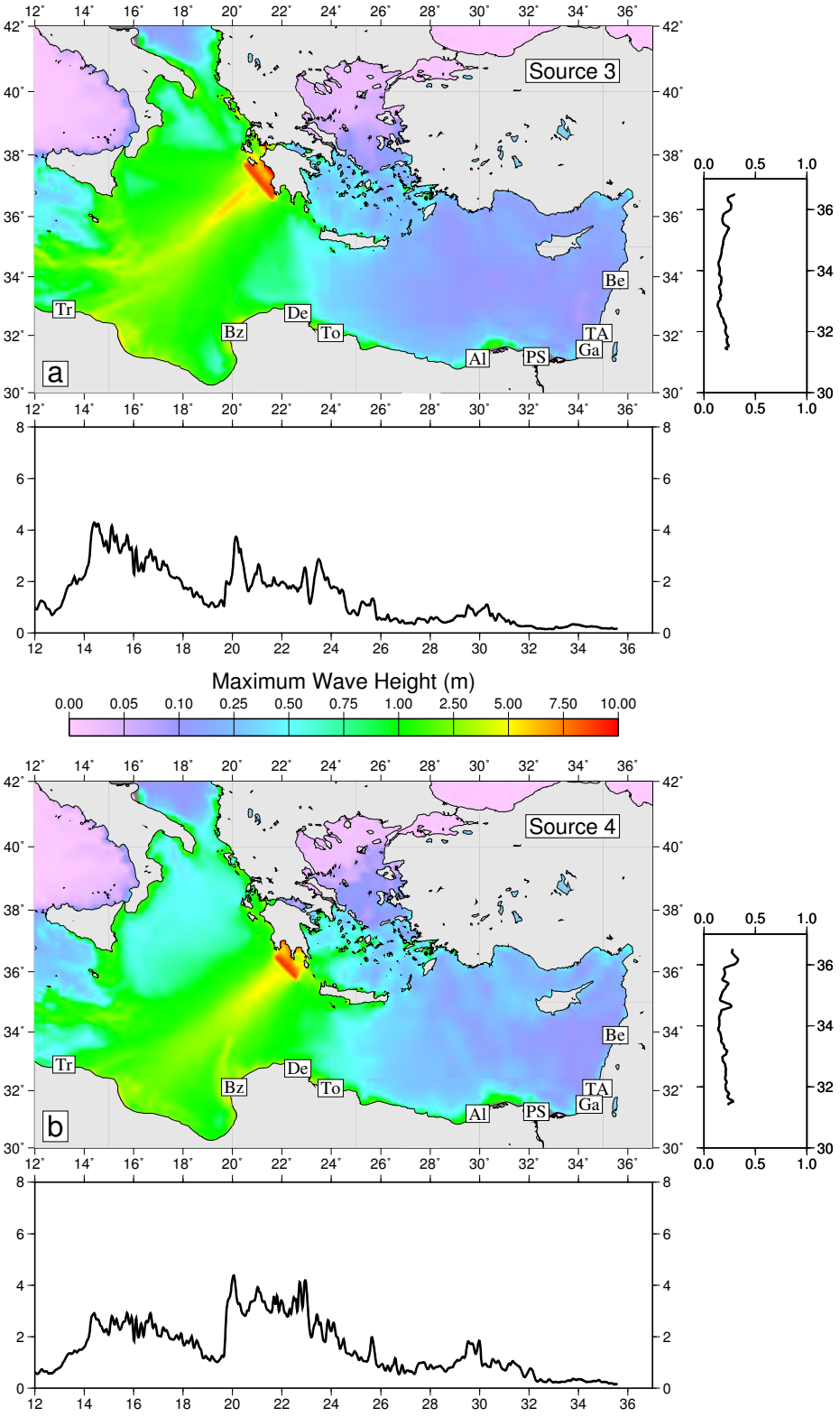

Figure 7. As Figure 6 for sources near the Peloponnese (Figure 5a).

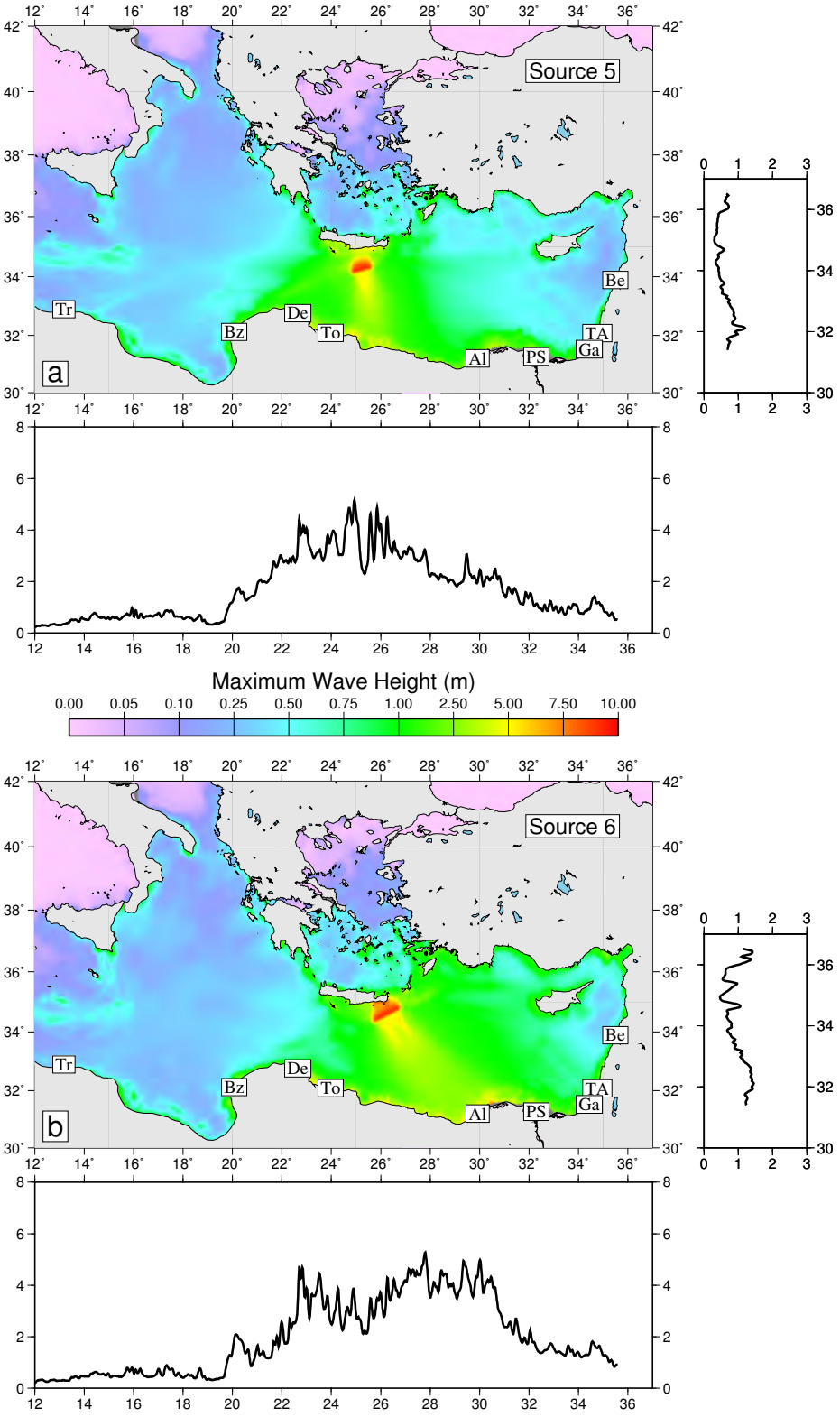

Figure 8. As Figure 7 for sources near eastern Crete (Figure 4).

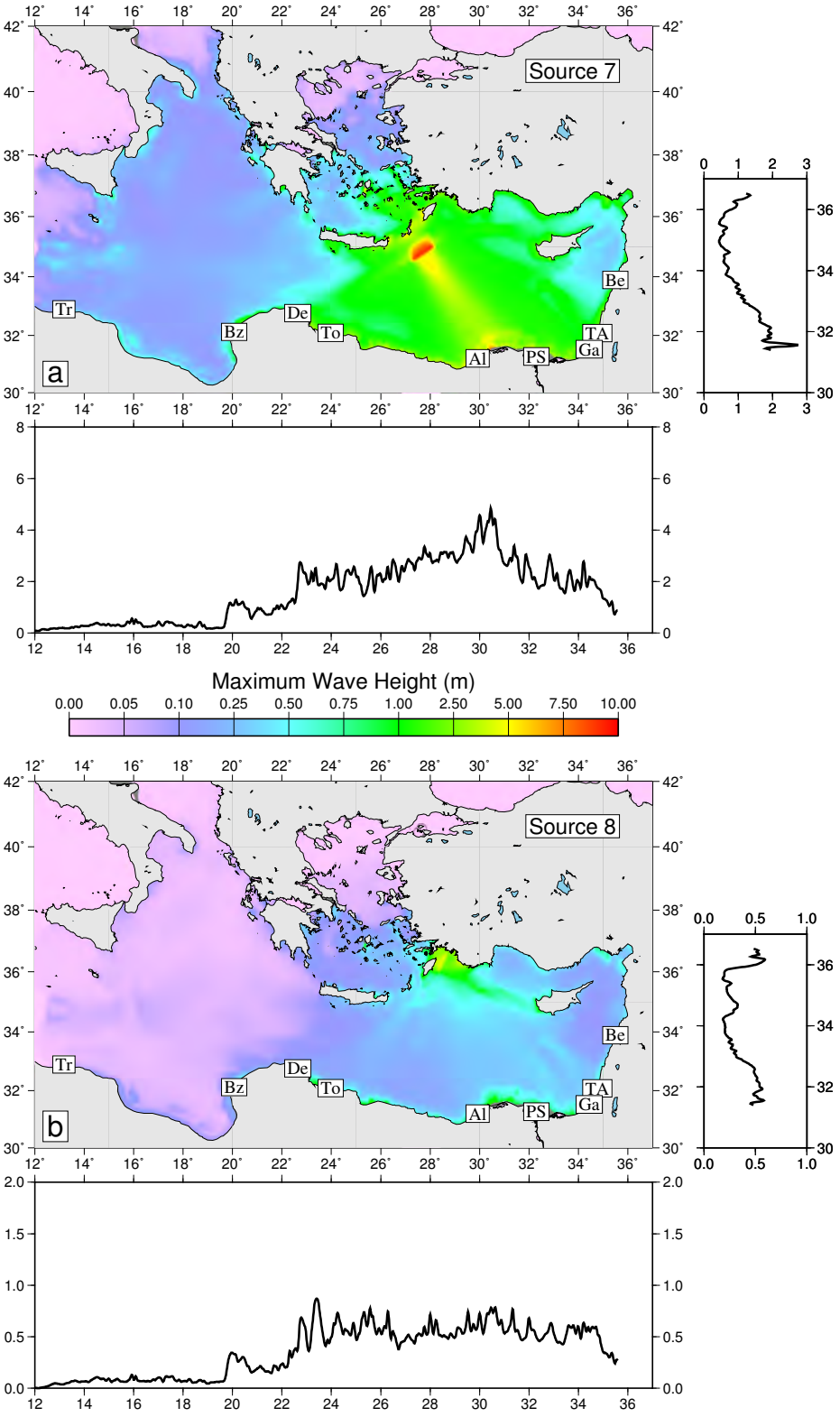

Figure 9. As Figure 7 for sources at the eastern end of the Hellenic plate boundary (Figure 5b.)

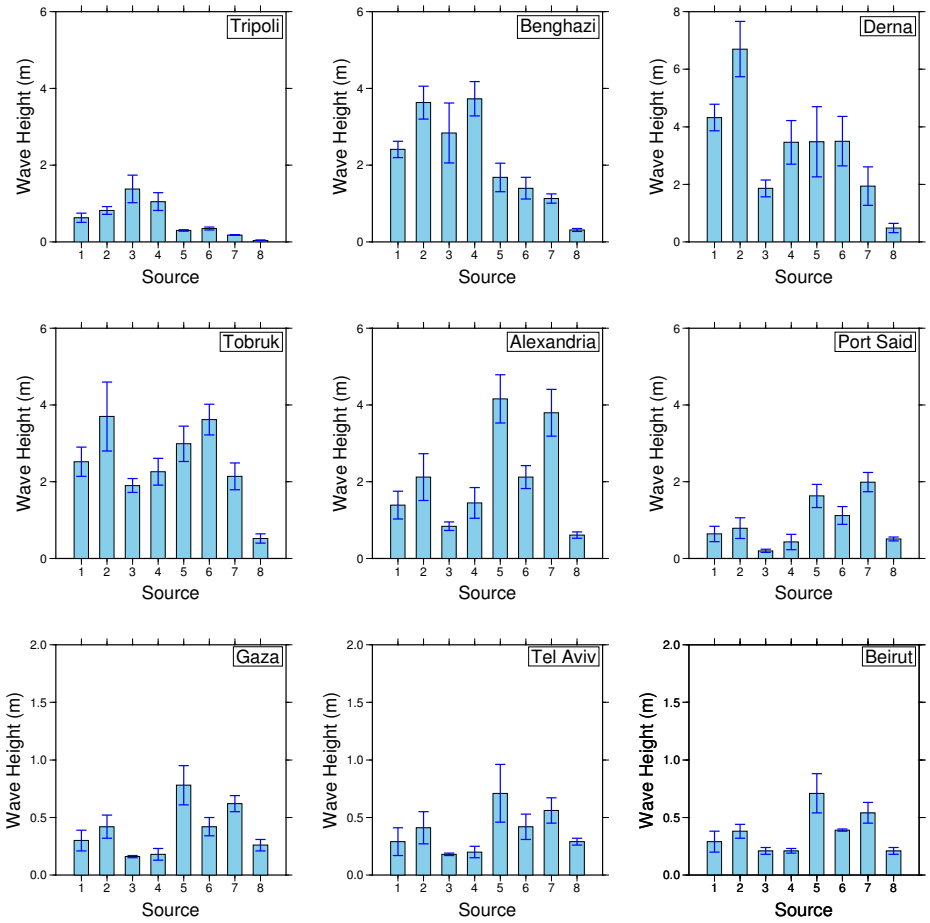

Figure 10. Maximum calculated wave heights at the 50-m isobath near large cities on the coasts of North Africa and the Levant for the eight tsunami sources illustrated in Figures 6 to 9. Bars show the average of the maximum waveheight for the points on the 50-m isobath within 25 km of the city; error symbols show the range of ± 2 standard deviations in those measurements. Note that the vertical scales differ. These calculations can not be used to make estimates of run-up and inundation, however calculated wave heights of over 1m indicate the possibility of substantial flooding.